Microclimate temperature variations from boreal forests to the tundra

Juha Aalto[1,2]*, Vilna Tyystjärvi[1,2], Pekka Niittynen[2], Julia Kemppinen[3], Tuuli Rissanen[2], Hilppa Gregow[1], Miska Luoto[2]

[1]Finnish Meteorological Institute, P.O. Box 503, FI-00101 Helsinki, Finland.

[2]Department of Geosciences and Geography, University of Helsinki, P.O. Box 64, Gustaf Hällströmin katu 2a, FI-00014 Helsinki, Finland.

[3]The Geography Research Unit, University of Oulu, P.O.Box 8000 FI-90014, Oulu, Finland.

*Corresponding author: Juha Aalto (juha.aalto@fmi.fi)

ORCIDs: Juha Aalto: 0000-0001-6819-4911; Vilna Tyystjärvi: 0000-0002-1175-5463; Pekka Niittynen: 0000-0002-7290-029X; Julia Kemppinen: 0000-0001-7521-7229; Tuuli Rissanen: 0000-0001-9912-4676; Hilppa Gregow: 0000-0003-3805-2247; Miska Luoto: 0000-0001-6203-5143

Abstract

Microclimate varies greatly over short horizontal and vertical distances, and timescales. This multi-level heterogeneity influences terrestrial biodiversity and ecosystem functions by determining the ambient environment where organisms live in. Fine-scale heterogeneity in microclimate temperatures is driven by local topography, land and water cover, snow, and soil characteristics. However, their relative influence over boreal and tundra biomes and in different seasons, has not been comprehensively quantified. Here, we aim to 1) quantify temperature variations measured at three heights: soil (-6 cm), near-surface (15 cm) and air (150 cm), and

25 2) determine the relative influence of the environmental variables in driving thermal variability.

26 We measured temperature at 446 sites within seven focus areas covering large macroclimatic,

27 topographic, and ecosystem gradients (tundra, mires, forests) of northern Europe. Our data,

28 consisting of over 60 million temperature readings during the study period of 2019/11-2020/10,

29 reveal substantial thermal variability within and across the focus areas. Near-surface

30 temperatures in the tundra showed the greatest instantaneous differences within a given focus

31 area (32.3°C) while the corresponding differences for soil temperatures ranged from 10.0°C

32 (middle boreal forest) to 27.1°C (tundra). Instantaneous differences in wintertime air

33 temperatures were the largest in the tundra (up to 25.6°C, median 4.2°C), while in summer the

34 differences were largest in the southern boreal forest (13.1°C, median 4.8°C). Statistical

35 analyses indicate that monthly-aggregated temperature variations in boreal forests are closely

36 linked to water bodies, wetlands, and canopy cover, whereas in the tundra, variation was linked

37 to elevation, topographic solar radiation, and snow cover. The results provide new

38 understanding on the magnitude of microclimate temperature variability and its seasonal

39 drivers and will help to project local impacts of climate change on boreal forest and tundra

40 ecosystems.

41 Key words

42 surface temperature; soil temperature; air temperature; wetlands; thermal heterogeneity

1. Introduction

Boreal forest and tundra biomes cover one third of Earth's terrestrial surface and are experiencing rapid climatic warming with severe consequences (Post et al. 2009). These high-latitude biomes also play a key role in the global climate system, storing an estimated 50% of global soil carbon (McGuire et al., 2009; Virkkala et al., 2021). The warming trend is projected to continue during the upcoming decades with the most pronounced changes projected to occur during the winter season (Ruosteenoja et al. 2016, 2019; Bintanja and Andry, 2017). To track these changes and their impacts, climate change research heavily relies on coarse-gridded macroclimate data (Flato, 2011; Bedia et al., 2013; Lenoir et al., 2013; Gardner et al., 2019). However, local climate conditions can differ substantially from those represented by these macroclimatic temperature grids (e.g., Lembrechts et al., 2019; Haesen et al., 2021). Thus, recently there has been a renewed focus on microclimate owing to its paramount importance in understanding how organisms and ecosystems respond to climate change (Potter et al., 2013; De Frenne et al., 2021).

The impact of macroclimate on ecosystems is filtered through physiographic, edaphic, and biotic characteristics of the landscape (Ashcroft and Gollan, 2013; Lenoir et al., 2017). These microclimatic drivers alter air mixing, heat transfer and budgets of short- and long-wave radiation, that potentially lead to contrasting wind, thermal, and humidity conditions within short horizontal and vertical distances (Barry and Blanken, 2016). Further, these conditions create microclimates where local temperatures can considerably differ from the macroclimate (Dobrowski, 2011; Graae et al., 2012; De Frenne et al., 2019). In terrestrial biomes, microclimate influences species distributions, biodiversity, and ecosystem functions by determining ambient temperatures for near-surface and soil organisms, and consequently, further influences productivity, decomposition, and carbon cycling (Greiser et al., 2018;

68 Lembrechts et al., 2019; Niittynen et al., 2020; Zellweger et al., 2020; Seibold et at., 2021).

69 Thus, understanding the magnitude of thermal differences in a landscape at a given time (i.e.,

70 thermal heterogeneity; Scherrer and Körner, 2011; Lenoir et al., 2013), and the relative

71 contributions of static landscape factors (e.g., topography) and dynamic factors (e.g., canopy

72 closure and snow cover) driving thermal heterogeneity is needed for projecting how climate

73 change shapes ecosystems.

74

75 In boreal forests, canopy intercepts radiation (both incoming and outgoing), decelerates air

76 flow, and affects evapotranspiration, thus creates microclimates where temperature variation is

77 buffered compared to macroclimatic temperatures outside the canopy (Barry and Blanken,

78 2016; De Frenne et al., 2021). In contrast, microclimatic temperature variability may be

79 accentuated compared to macroclimate in areas that are exposed to high radiation, sheltered

80 from winds, and have dry soils. Vegetation drives microclimatic temperature variability also

81 in the tundra (Aalto et al. 2013; Kemppinen et al. 2021). There, the role of local topography is

82 expected to be especially strong due to its influence on fine-scale variation in snow

83 accumulation, surface flow, net radiation, and cold-air pooling under stable atmospheric

84 conditions (Pepin et al., 2009; Daly et al., 2010; Aalto et al., 2017; Niittynen et al., 2020). Local

85 hydrology also influences microclimate temperatures due to the high specific heat capacity of

86 water. This can lead to buffered temperatures in areas with high soil moisture and in areas near

87 wetlands and water bodies (Yang et al., 2012; Ashcroft and Gollan, 2013; Słowińska et al.

88 2022.).

89

90 In addition to various environmental drivers, microclimate temperature also depends on the

91 height from the surface (Barry and Blanken, 2016). In general, temperature variations are

92 largest close to the surface, and decrease with height due to increased air mixing. Below

93 ground, temperature variability is buffered compared to above soil surface temperatures and is

94 controlled by soil heat flux. This, in turn, is driven by surface radiation balance, specific heat

95 capacity of the soil (dependent on e.g., soil moisture), and seasonal snow cover that effectively

96 insulates the ground from temperature fluctuations in the free air (Grundstein et al., 2005; Aalto

97 et al., 2018, Fernández-Pascual and Correia-Álvarez, 2021). These vertical variations in

98 microclimate temperatures are also relevant for different ecosystem functions. For example,

99 soil temperatures are closely linked to e.g., soil respiration and nutrient cycling via controlling

100 microbial activity and mycorrhiza associations (Soudzilovskaia et al., 2015; Du et al., 2020).

101 In turn, air temperatures close to the surface are especially relevant for animals living on the

102 surface or in the litter, plant ecophysiology and metabolism, and decomposition (Körner and

103 Hiltbrunner, 2018; Seibold et al., 2021). Air temperature measured 1–2 m above the soil surface

104 represents conditions relevant for larger organisms and ecosystem-level processes, such as

105 local productivity patterns (Potter et al., 2013). However, standardized weather stations and

106 gridded climate datasets (e.g., Fick and Hijmans, 2017; Karger et al., 2017) often ignore the

107 vertical temperature gradients and consequently misrepresent local climate conditions relevant

108 for many organisms and ecosystem processes (Suggitt et al., 2011; Graae et al., 2012; De

109 Frenne and Verheyen, 2016).

110

111 The relative importance of microclimate temperature drivers can substantially differ across and

112 within biomes (Barry and Blanken, 2016). However, in the past, most empirical microclimate

113 studies have been conducted over single study settings with limited spatial extents (e.g., Pepin

114 et al., 2009; Yang et al., 2012). Therefore, the understanding of the thermal characteristics

115 across biomes and their contributing factors has remained limited. Here, we investigate

116 microclimate temperature variation at various heights using a dense network of microclimate

117 stations over a large geographical extent. More precisely, we aim to 1) quantify the temperature

118   variability measured at three heights: soil (-6 cm), near-surface (15 cm) and air (150 cm), and

119   2) examine the relative influence of the environmental variables driving spatio-temporal

120   variation of the temperature parameters. The study is based on a large network of miniature

121   and low-cost microclimate stations installed at study sites (n=446) within seven focus

122   landscapes (hereafter focus areas) located in northern Europe. The study domain covers large

123   gradients of macroclimate and elevation, and distinct ecosystems from both the boreal forest

124   and tundra biomes.

125

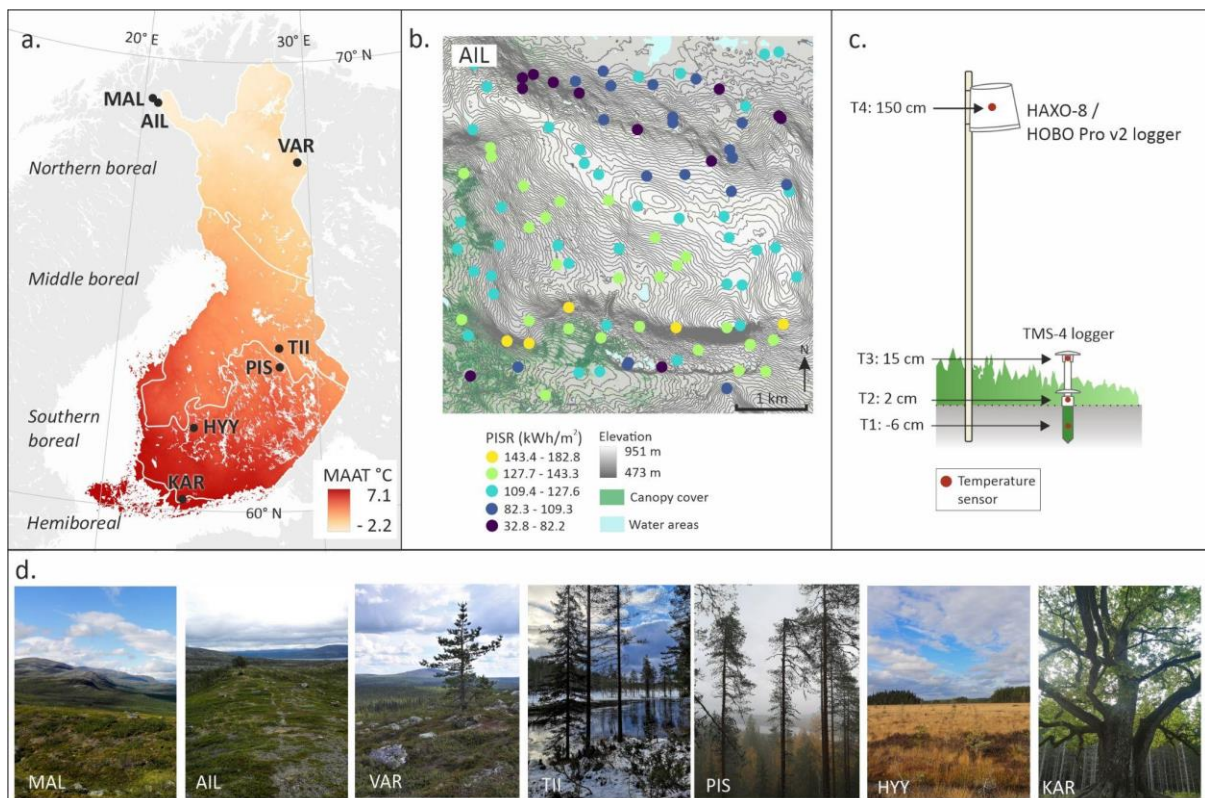126   2. Material and methods

127   **2.1. Study domain and design**

128   The study domain extends across seven focus areas in Finland from hemiboreal forests to the

129   oroarctic tundra and covers large gradients in macroclimate, elevation, and ecosystems (Fig 1).

130   Climate in Finland is highly influenced by the Polar Front as well as the North Atlantic Current

131   which drive macroclimatic temperature and precipitation patterns. These are also influenced

132   by the Scandes mountains in the west and the landmass of the Eurasian continent in the east

133   (Tikkanen, 2005). Along the latitudinal gradient of ca. 60–69 N, mean annual air temperatures

134   range from -2.2°C to 7.1°C (1991–2020 period, Jokinen et al., 2021). The elevational gradient

135   of the study domain ranges from ca. 30 to 950 meters above sea level with pronounced local

136   and regional topographical variation due to multiple past glaciations. Moreover, due to the

137   glaciations and the relatively humid climate, lakes and mires are abundant in Finland

138   (Tikkanen, 2005).

139

140   The selected focus areas are mainly situated in protected areas to minimize the influence of

141   anthropogenic disturbance. Each focus area has 50–100 microclimate stations at which loggers

142   were installed to measure soil and air temperature (see Table 1; Fig S1 and section 2.3. for

more details). The northernmost focus areas are in Kilpisjärvi, north-western Finland, around Mount Malla and the Malla nature reserve (hereafter, MAL) and Mount Ailakkavaara (AIL). Another focus area in northern Finland is located in the Värriö nature reserve (VAR) in Salla and Savukoski, in the north-east. All the three northernmost areas have measurement sites above and below the forest line, and they are characterized by the boreal forest - tundra ecotone differentiating them from the central and southern areas. In central Finland, two focus areas are located within and around the Pisa nature reserve (PIS) in Kuopio and within the Tiilikkajärvi national park (TII) in Rautavaara. PIS is characterized by boreal forests and varying topography whereas TII comprises mainly mires. Another focus area characterized by mires is the Hyytiälä region (HYY) in southern Finland, where the stations are located within and nearby the Siikaneva nature reserve. The southernmost focus area is located within the Karkali nature reserve (KAR) and other nearby protected areas in Lohja, in the hemiboreal zone.

158 **Figure 1. Study domain and design.** Panel **a** represents the locations of the seven focus areas

159 in relation to the mean annual air temperature in Finland (MAAT; 1991–2020). The white

160 borders mark boreal vegetation zones (in italics). White polygons represent water bodies over

161 10 km². Northernmost focus areas (MAL, AIL, VAR) are in the boreal forest–tundra ecotone

162 comprising both northern boreal forests and oroarctic tundra. Panel **b** represents an example of

163 the sampling design in AIL with the colored points depicting annual potential incoming solar

164 radiation (PISR) calculated from a digital elevation model. Panel **c** depicts the logger placement

165 and measurement heights (T1=soil, T2=surface, T3=near-surface, T4=air) at the microclimate

166 stations**.** T2 was only used to derive snow cover information (see Material and methods for

167 details). Field photos from each focus area are presented in panel **d**. Focus area abbreviations

168 are defined in the main text and in Table 1.

169

170 To determine the measurement sites, we conducted a random stratification to pre-select a suite

171 of candidate locations that maximally cover the main environmental gradients within the focus

172 areas (Fig S2). This was done separately for each focus area. The stratification was based on

173 several variables e.g., total canopy cover, deciduous canopy cover, distance to forest edge,

174 elevation, potential annual incoming solar radiation, and a topographic wetness index (the

175 SAGA wetness index), although the final selection of the variables varied depending on the

176 distinct features of each area. First, we masked the areas outside the nature reservations and

177 extracted the remaining pixel information on a systematic grid with a 10-m cell size. Next, we

178 randomly selected 50% of the points and used this subset to reduce the multidimensional

179 environmental space into its first three principal components. Then we took a sub-sample of

180 100 points that maximally and systematically covered the shrinked environmental space. We

181 repeated these procedures 100 times and used the selection frequency for each point as a weight

182 in the final random point selection. This two-step selection process was also necessary to be

able to ascertain a minimum distance (100m) between the selected points to avoid

pseudoreplication. These steps used the eSample function from iSDM R package (Hattab and

Lenoir 2017). Using such a protocol, we were able to detect (and select) the points that are

unique in terms of their environmental conditions and thus likely valuable locations in the

station network. Selected points were visually inspected by examining the environmental

variables' distributions. Final judgment of each preselected location was confirmed at the field.

Table 1. Description of the seven focus areas. Mean annual air temperature data for 1991–
2020 are from Jokinen et al. (2021), and automated weather station data (AWS; Table S1) were
acquired for each focus area for the period of the microclimate measurements (2019/11/01-
2020/10/31).

| | Focus area | | Measurement setting | | | | | Mean air temperature (°C) | |
	Name	Center coordinate	Sites (n)	Logger	Area (km²)	Elevation (m)	Ecosystem	Annual 1991-2020	2019/11/01 - 2020/10/31
Northern Finland	**MAL:** Mount Malla, Malla nature reserve	69.071 N, 20.698 E	100	TMS-4 HOBO	23.8	482-934	Northern boreal forest - Tundra	-1.4	-0.7
	AIL: Mount Ailakkavaara	68.991 N, 21.015 E	100	TMS-4 HOBO	24.0	509-933	Northern boreal forest - Tundra	-1.4	-0.7
	VAR: Värriö nature reserve	67.736 N, 29.596 E	50	TMS-4 HAXO-8	22.7	262-475	Northern boreal forest - Tundra	0.1	1.1
Central Finland	**TII:** Tiilikkajärvi national park	63.646 N, 28.312 E	50	TMS-4 HAXO-8	17.7	187-205	Middle boreal forest	2.6	4.7
	PIS: Pisa nature reserve	63.218 N, 28.328 E	50	TMS-4 HAXO-8	16.0	103-262	Southern boreal forest	2.9	4.4
Southern Finland	**HYY:** Hyytiälä, Siikaneva nature reserve and nearby areas	61.831 N, 24.196 E	50	TMS-4 HAXO-8	51.5	152-203	Southern boreal forest	4.1	5.9
	KAR: Karkali nature reserve and surrounding protected areas	60.248 N, 23.830 E	50	TMS-4 HAXO-8	47.5	32-99	Hemiboreal forest	6.0	7.9

2.2. Weather station data

Hourly weather station data for the study period of 2019/11/01–2020/10/31 and long-term averaged climate data for the years 1991–2020, was acquired from each focus area's nearest automated weather station (AWS) operated by the Finnish Meteorological Institute (Fig S3; Table S1). The data have undergone an operational quality control.

2.3. Microclimate temperature data

All microclimate stations were equipped with a Tomst TMS-4 logger (Wild et al., 2019) and either a LogTag HAXO-8 (LogTag North America Inc.) or Onset HOBO U23 Pro v2 logger (Onset Computer Corporation; with exceptions of Ailakkavaara and Malla study areas which both have 100 TMS-4 loggers and 40 HAXO/HOBO loggers). The TMS-4 temperature sensors measure temperature at three heights (Fig 1c): -6 cm for soil temperature (T1), 2 cm for surface temperature (T2), and 15 cm for near-surface temperature (T3) with a precision of 0.0625°C and an accuracy of ± 0.5°C. Noteworthy, in this study, T2 is used only for interpreting snow cover duration from the surface temperature values. Additionally, TMS-4 also measures soil moisture, which is used in this study as a predictor of microclimate temperature variation (see sections 2.5. and 2.7.). We measured air temperature at 150 cm (T4) by using HAXO-8 (precision of 0.1°C; accuracy ±0.3°C for ambient temperatures of 0°C-50°C and ±0.6°C for ambient temperatures below 0°C) and HOBO loggers (precision 0.04°C; accuracy ±0.2°C from 0 to 70°C and ±0.25 from -40 to 0°C). These sensors were installed under white well-ventilated plastic radiation shields on the north side of either tree trunks or wooden poles to reduce exposure to direct solar radiation. Both sensors also measure air humidity, which was used only as a part of the data quality control in this study (see Section 2.4.). TMS-4 loggers were set to log at 15-minute, HOBO loggers at 30-minute, and HAXO loggers at 2-hour intervals due to different memory capacities of the loggers. To keep the 150 cm air temperature measurements

220 comparable between the two logger types, we thinned the HOBO time series to the matching

221 2-h intervals of the HAXO loggers. The stations were installed in June-October 2019. The

222 study period is one year from 2019/11/01 to 2020/10/31 which is fully covered in all the study

223 areas.

224

225 **2.4. Data preprocessing and quality control**

226 All temperature time series were visually quality checked. If, for instance, a logger had fallen

227 down or its radiation shield was detached, such time periods were identified, and the

228 jeopardized measurements were removed. Additionally, four sources of error were detected

229 and corrected: 1) sensors systematically recording too low or high temperatures, 2) erroneous

230 peaks over one or few consecutive measurements, 3) HAXO and HOBO loggers skipping

231 measurements but continuing to count the time after the gap from the last timestamp before the

232 failure, thus disengaging the correct time and temperature, and 4) snow reaching the height of

233 the HAXO and HOBO loggers (T4, 150 cm). We created the following automated procedures

234 to correct these issues. The R code used for these steps can be found in the public focus area -

235 specific Github repositories under user *Poniitty* (e.g., the raw data and processing code for

236 VAR in https://github.com/poniitty/varrio_microclimate).

237

238 1) We identified the periods when the TMS-4 loggers were "out-of-field" at stable conditions

239 (no temporal variation). We calculated the mean temperature of these periods for each sensor

240 and compared these means across the three sensors within each logger. We arranged the sensors

241 based on these means and corrected the sensors recording the highest and lowest mean

242 temperatures to match with the middle one. Then, we used these correction temperatures to

243 correct for systematic deviations over the whole sensor-specific time series. These corrections

244 were mostly very minor (<0.1°C) but in some rare cases even as high as 0.5°C. Thus, the

245 corrections were considered to greatly improve the reliability of the dataset.

246

247 2) To automatically detect erroneous peaks in the TMS-4 data, we iterated over all individual

248 time series month by month and detected the logger within the same study area that best

249 matched with the temporal pattern of the focal sensor (in terms of highest pairwise correlation

250 and lowest root mean-squared error, RMSE). We then calculated moving averages and

251 identified moments when the successive measurements showed a large rise or drop and when

252 the two loggers showed suspicious differences based on the calculated statistics. By careful

253 inspection, we set multiple criteria and thresholds for the differences to judge whether the peak

254 in temperatures was a result of a natural event or an error. Erroneous peaks and their adjacent

255 measurements were removed and replaced by linear interpolation while taking the

256 measurements of the matching sensor into account as well.

257

258 3) To correct for non-matching timestamps in the HOBO and HAXO data (T4), we calculated

259 a median time series over all other loggers within each study area to which the individual logger

260 time series were compared to. We calculated running correlations and identified breakpoints

261 when the reference time series and a focal logger time series started to deviate from each other.

262 If a breakpoint was identified, we started to gradually shift the temperature measurements of

263 the focal logger and moved the post-breaking point data to a period where it reached maximum

264 correlation with the reference period. We repeated this procedure multiple times to find all

265 potential breaking points and to trim the gap margins efficiently. The outcomes were visually

266 inspected to see if further corrections were needed (see an example of a corrected time series

267 in Fig S4).

268

269   4) We identified periods when the HAXO/HOBO loggers were under snow by calculating

270   variability and extremes of temperature and relative humidity from individual time series with

271   a 5-days moving window. We selected multiple criteria (e.g., low temporal variability,

272   maximum temperatures <0.5°C) to find the potential periods of snow coverage and if these

273   conditions persisted for several consecutive days the measurements were removed from the

274   dataset. After quality checks temperature data from 446 study sites was used in the analyses

275   but the number varies by month and measuring height (see details in Fig S5).

276

277   The deployed radiation shielding has an effect on the temperature readings as the shield itself

278   is likely to affect measured temperatures, and consequently, the accuracy of the measurements

279   (Maclean et al., 2021). The effect is expected to be largest when direct sunlight is at its strongest

280   (during solar noon and summer solstice) and wind speed is low. In the north where the solar

281   angle is relatively low, early summer measurements can be affected by reflected short-wave

282   radiation from the snow-covered surface. To mitigate these potential issues in our temperature

283   data, we defined maximum temperatures (annual and summer) as the 95th percentiles of

284   individual time series. In addition, T2 measurements that represent surface temperatures (Fig

285   1c) can be problematic since the proper installation height (+2 cm) is difficult to estimate in

286   the field, particularly in areas with herbaceous vegetation and bryophytes. Therefore, we

287   present the results of T1, T3 and T4 in the main text, and use T2 temperature data only to

288   calculate periods of snow cover (see 2.5.).

289

290   **2.5. Soil moisture and snow cover**

291   We used monthly soil moisture as a predictor of monthly microclimate temperatures (see 2.7.).

292   Mean monthly soil moisture was calculated from the TMS-4 loggers. The loggers measure soil

293   moisture in the upper 15 cm soil layer and the raw soil moisture count values were transformed

294 to volumetric water content (VWC%) with a calibration function adopted from Wild et al.

295 (2021). Soil moisture measurements were considered only when soil temperature of the same

296 logger was above 1°C. To impute soil moisture for the missing months (mainly in winter), we

297 used the value of the last month with sufficient soil moisture data. If this was not possible, we

298 modeled the local soil moisture based on measurements at the focal site of other years (2019–

299 2021) and all data from all other loggers within the study area by fitting a linear mixed effect

300 model, in which we included the month and year as factor predictors and the study site as a

301 random factor. This model was then used for predicting the missing monthly values.

302

303 Snow cover duration was also used for predicting monthly microclimate temperatures (see

304 Section 2.7.). It was determined from the surface temperatures (T2) of the TMS-4 loggers by

305 counting the days when the maximum surface temperature stayed below 1°C and the diurnal

306 temperature range was below 10°C calculated with a 10-day moving average. The outcome

307 was visually checked, and the algorithm was considered to detect periods of snow cover well

308 in general. We identified three wetland study sites in the TII study area where the top peat layer

309 stayed so warm under the snow that the automatic snow cover detection failed. For these sites,

310 we identified the snow-covered period visually from the temperature time series. Missing

311 values in snow cover duration were imputed in a similar way to the soil moisture values with

312 the following differences: a generalized linear mixed effect model was used with Poisson

313 distribution and only year was included as a factor predictor. The exact method and code to

314 calculate the snow cover duration are available at the study-area-specific Github repositories

315 (https://github.com/poniitty?tab=repositories).

316

2.6. Geospatial data

We utilized a multitude of geospatial datasets to derive variables that represent the major environmental drivers hypothesized to affect microclimate temperatures in boreal and tundra biomes. We used airborne light detection and ranging (LiDAR) data, which was provided by the National Land Survey of Finland (https://www.maanmittauslaitos.fi/en/maps-and-spatial-data/expert-users/product-descriptions/laser-scanning-data). The LiDAR data was collected over summers 2016-2019. The point density is ~0.5p/m^2, the standard error of the elevation accuracy is at maximum 15 cm, and the standard error in horizontal accuracy 60 cm. We downloaded a canopy height model produced by the Finnish Forest Center at 1-m spatial resolution (https://www.metsakeskus.fi/fi/avoin-metsa-ja-luontotieto/aineistot-paikkatieto-ohjelmille/paikkatietoaineistot). It is based on the same LiDAR datasets introduced above. We also downloaded and utilized the Finnish national Topographic database which contains e.g., all water bodies, rivers, and wetlands in vector format (https://www.maanmittauslaitos.fi/en/maps-and-spatial-data/expert-users/product-descriptions/topographic-database).

We constructed eight predictors that represent the main aspects of topography, solar radiation, vegetation, and land cover types that are known to affect microclimate temperature (e.g., Ashcroft and Gollan, 2013; Aalto et al., 2017; Greiser et al., 2018). Topographic predictors, i.e., elevation, potential incoming solar radiation (PISR), and topographic position index (TPI), represent the available energy and cold air pooling capacity. Vegetation effects were represented by canopy cover as high and dense vegetation shades the ground and slows down air movement. Wetland and water body proportions in the surroundings were included to represent their potential buffering effect on temperatures. Additionally, we included the mean soil moisture and snow cover duration calculated from the TMS-4 loggers as predictors.

342

343 A Digital Terrain Model (DTM) was produced for each study area based on the LiDAR datasets

344 using the grid_terrain function from the lidR R library (Roussel et al., 2020). The DTM

345 represents elevation at 2-m spatial resolution. These DTMs were then used to calculate

346 potential incoming solar radiation (PISR) for the 15th day of each calendar month using the

347 Potential Incoming Solar Radiation tool in the SAGA-GIS software (version 7.6.2;

348 http://www.saga-gis.org/saga_tool_doc/7.6.2/ta_lighting_2.html). TPI describes the difference

349 in elevation between a focal location and the mean surrounding elevation which we defined

350 with a 100-m radius. TPI was calculated using the Topographic Position Index tool in SAGA-

351 GIS (http://www.saga-gis.org/saga_tool_doc/7.6.2/ta_morphometry_18.html). Canopy cover

352 was calculated from the canopy height model as a proportion of vegetation higher than two

353 meters within a five-meter buffer around the focal location. We extracted still water bodies and

354 wetland land cover polygons from the topographic database (scale 1:10 000), and then

355 calculated the proportion of these land cover types using a 1000 m or 100 m buffer respectively

356 for each logger location.

357

358 **2.7. Statistical modeling of monthly microclimate temperatures**

359 We used multivariate statistical modeling to investigate environmental drivers of the monthly

360 microclimate temperatures, as detailed below:

361

362 **Response variables.** We aggregated the quality-checked temperature time series to monthly

363 means (Tavg), maximums (Tmax) and minimums (Tmin). We used the 95th percentile to

364 calculate Tmax, as we expected this to dilute the potential effect of unrealistically high

365 individual measurements caused by the radiation shield. The three measurement heights (i.e.,

366   T1, T3, T4), three summary statistics (Tavg, Tmax, Tmin), and 12 months led to a total of 108

367   response variables.

368

369   **Predictors.** We included the eight predictors (i.e., elevation, PISR, TPI, canopy cover,

370   wetlands, waterbodies, mean soil moisture and snow cover duration) in the models to explain

371   variation in the response variables. However, as the conditions of the seven focus areas contrast

372   greatly, we used a slightly different set of predictors for each area to facilitate model realism.

373   For example, in winter 2019–2020 there was no permanent snow cover in Southern Finland

374   and thus the snow variable was omitted in the model of KAR. Snow cover was also omitted

375   from monthly models for other areas when all study locations were snow free for the whole

376   month. KAR, HYY, and TII show minimal variation in elevation (Table 1). From the initial

377   model results, we noticed that these short elevational gradients resulted in unrealistic model

378   estimates for elevation, and thus, it was omitted from the models for these areas. Furthermore,

379   the proportion of water bodies was not included in VAR, because this focus area has no lakes.

380   **Multivariate modeling.** We related the response variables to the predictors by fitting linear

381   models separately for each month and focus area. We considered only linear terms of the eight

382   predictors, because we did not expect strong nonlinear responses, and to avoid the risk of

383   overfitting. After running a full model with all the relevant predictors included, we ran a step

384   function to select the best model based on the AIC value with a both backward and forward

385   mode of stepwise search. As a measure of variable importance, we compared the explanatory

386   power (R^2) of the final model to a model in which the focal predictor was randomly permuted

387   with the vi function from vip R library (Greenwell and Boehmke, 2020). This function also

388   determines the direction of the effect for each predictor based on the sign of the t-statistic,

389   which is analogous to the sign of the slope parameter in regression analysis. If the permuted

390   predictor is important, the R^2 will drop greatly leading to a high importance value. The overall

391 explanatory power of the model is also reflected in the variable importance scores as the drop

392 in R^2 cannot be high if the R^2 is low in the first place. This also gives less weight for poorly

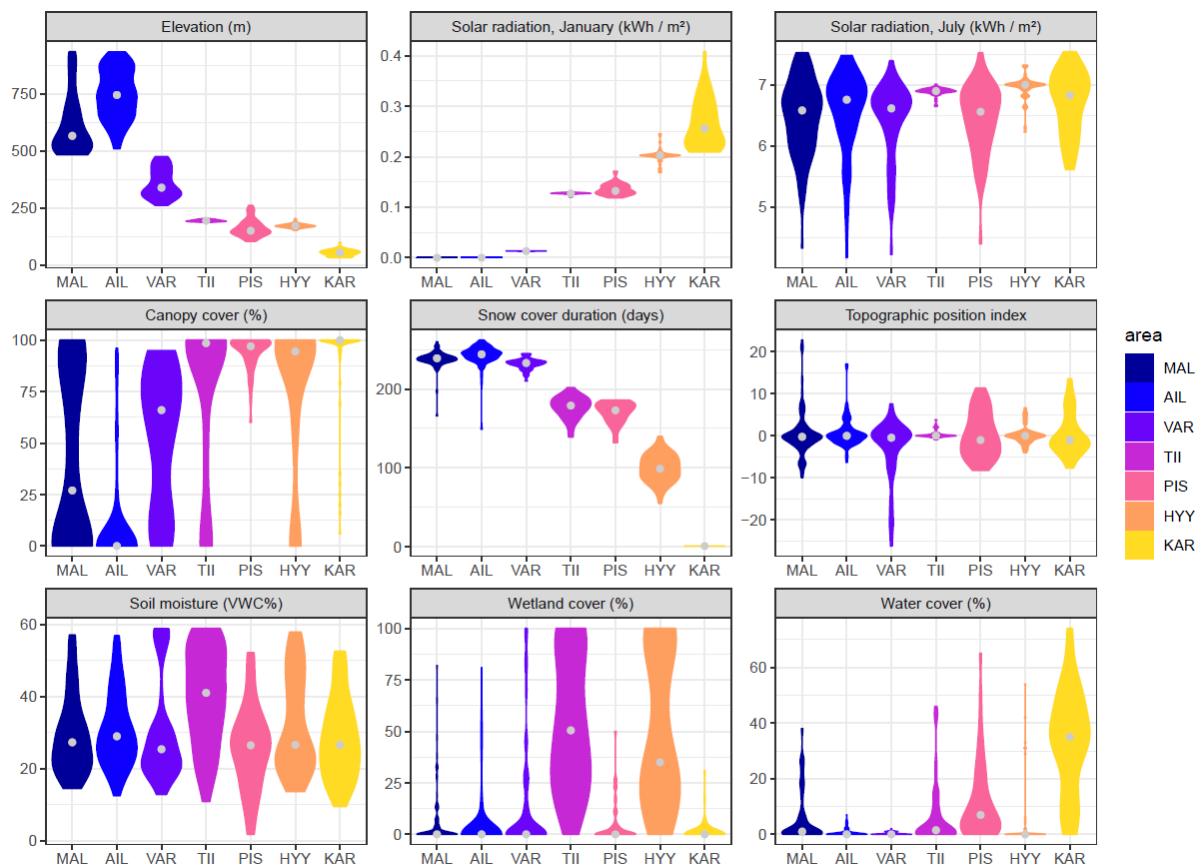393 performed models when the results are compared or summarized.

394

395 3. Results

396 **3.1. Environmental gradients**

397 Our microclimate station network across the seven focus areas covers large environmental

398 gradients (Fig 2; Table S2) with e.g., elevation ranging from 32 to 934 meters and snow cover

399 duration from 0 to 262 days (KAR to AIL). In most areas, canopy cover ranges from 0 to 100%.

400

401

402

403 **Figure 2. Environmental gradients covered by the microclimate station network.** The

404 figure represents the variability in environmental conditions within the seven focus areas (see
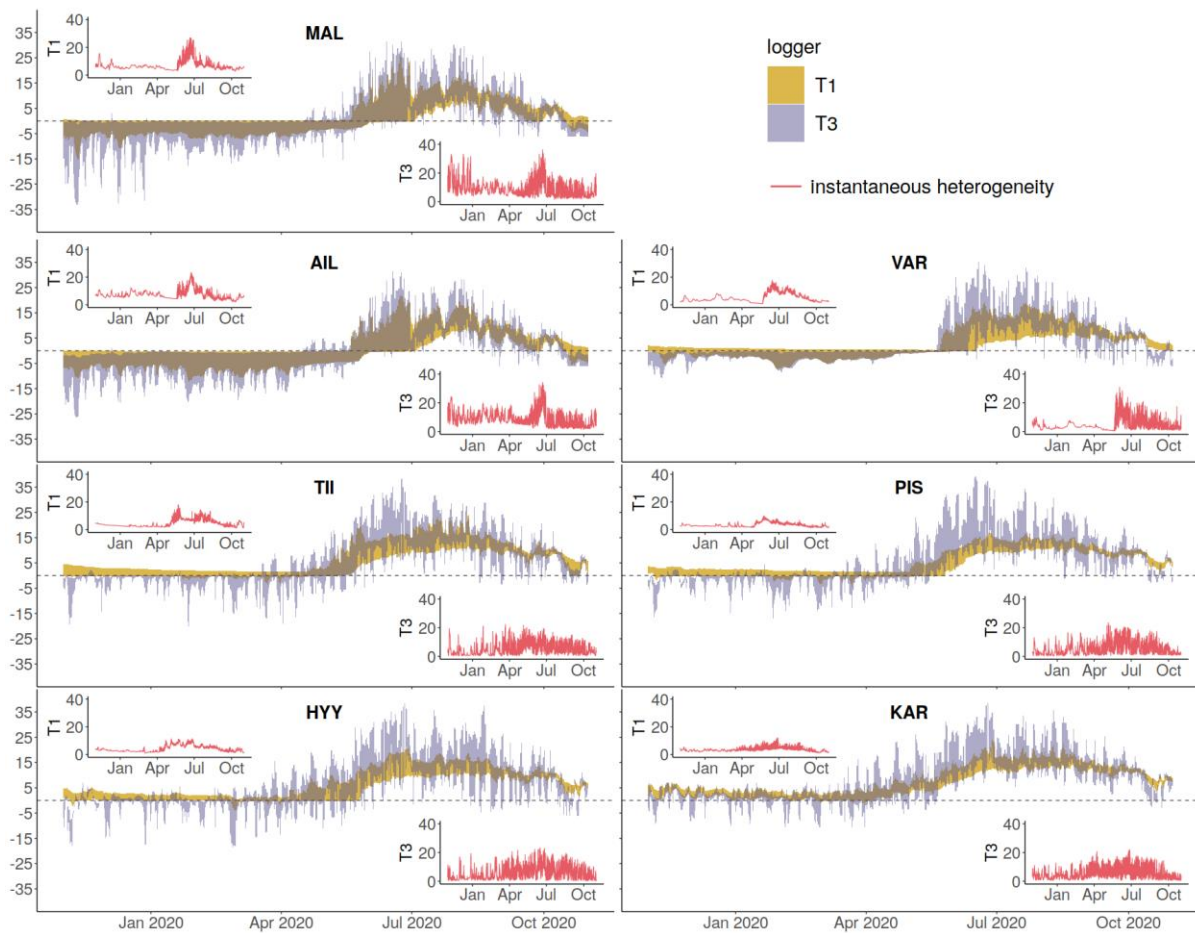
405   Table 1 for the abbreviations). Gray dots depict median values. These environmental variables

406   were used as predictors of the monthly microclimate temperatures.

407

408   **3.2. Spatio-temporal variability in microclimate temperatures**

409   The data demonstrate pronounced spatio-temporal variations in the microclimate temperatures

410   (Fig 3; Fig S6; Table 2). The intra-annual variation in near-surface (T3) and air temperatures

411   (T4) over all stations was large across the focus areas, for example 64.5°C and 69.3°C in MAL

412   (tundra), and 61.3°C and 54.7°C in HYY (southern-boreal forest), respectively. These

413   microclimate temperature variations often exceeded the variability measured by the adjacent

414   AWS (Table 2). In general, the amplitude of intra-annual soil temperature (T1) variation was

415   ca. 50% of the amplitude of T3 and T4 with the largest variation measured in tundra (ca.

416   42.1°C; MAL) and the smallest variation in the middle boreal forest (ca. 22.3°C; PIS). Spatial

417   variation in the microclimate temperatures was pronounced both within and among focus areas

418   as well as across seasons (Fig 4).

419

420
421

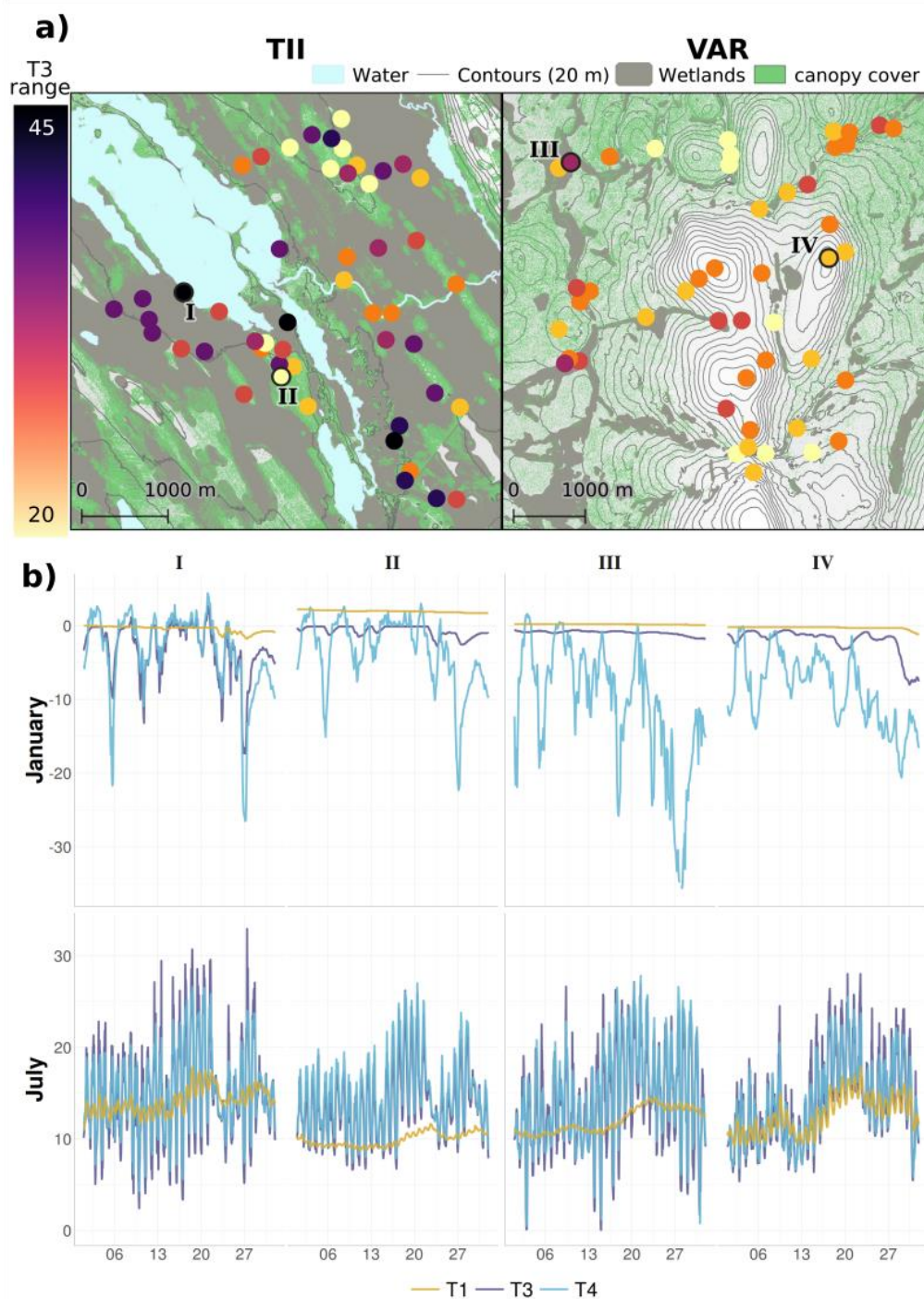**Figure 3. Spatio-temporal variability of soil and near-surface temperatures in the focus areas.** The polygons represent hourly temperature variability over the microclimate stations (number of stations 50–100 per focus area, see Table 1) at two heights, soil temperature (T1) and near-surface temperature (T3), over the study period 2019/11/01–2020/10/31. In the sub-panels, red lines show the maximum instantaneous temperature difference within a given focus area (i.e., thermal heterogeneity, numerical results in Table 2).

428

429

430

Figure 4. Microclimate temperature variability over two example focus areas. Panel **a** depicts intra-annual near-surface temperature (T3) variation over the microclimate stations in middle boreal forest (TII) and boreal forest-tundra (VAR). In TII, the intra-annual range in T3 was larger in open measurement sites (nearly 40°C), whereas in forested sites the variation was mostly below 30°C. In VAR, the largest intra-annual range in T3 was found in open wetland

areas (> 40°C), while areas with least annual variation were located either in forests or in depressions between fells (< 20°C). Canopy cover represents over 2 m heigh trees. Panel **b** shows January and July temperature time series from example microclimate stations (I–IV in panel **a**). The smallest temperature variations over both focus areas were found in forested sites (II and IV).

The results demonstrate large instantaneous, within-area thermal heterogeneity (Fig 3; Fig. S6; Table 2). For T3, the maximum instantaneous difference across all loggers within each focus area ranged from 17.8°C (KAR, median=3.3°C) to 32.3°C (MAL, 6.5°C). In the tundra, the largest within-area differences occurred mainly during the snowmelt season (late spring–early summer). In the southern focus areas (HYY and KAR), the magnitude of the thermal heterogeneity in T3 remained fairly constant throughout the year. Thermal heterogeneity in T1 was markedly suppressed during the snow cover period, especially in the northern focus areas (difference ranging from 7.3°C [MAL, median=5.1°C] to 12.4°C [AIL, 6.9°C]). The maximum instantaneous difference in T1 was largest in the tundra (27.1°C [MAL, 5.9°C] and 23.5°C [AIL, 6.7°C]) and smallest in the southern boreal zone (10.1°C in PIS, 2.9°C). Wintertime instantaneous differences in T4 were clearly largest in topographically heterogeneous tundra areas with the difference ranging from 17.5°C (AIL, 3.0°C) to 25.6°C (MAL, 4.2°C; Fig S6; Table 2). In contrast, during summer, maximum thermal heterogeneity was similar among the tundra and boreal focus areas, but the median heterogeneity was highest in the southernmost focus areas (HYY and KAR).

Table 2. Intra-annual temperature range of microclimate temperatures and thermal heterogeneity over each focus area. Temperature range over all microclimate stations within a focus area was determined for three measurement heights (T1, T3, and T4 for soil, near-

surface, and air temperatures, respectively) and adjacent automated weather stations (AWS). Instantaneous thermal heterogeneity depicts the maximum (median in brackets) within-area temperature difference at a given time.

| | Temperature range (°C) | | | | Instantaneuous thermal heterogeneity (°C) | | | | | | | | |
| | Intra-annual | | | | Annual | | | January | | | July | | |
Area	T1	T3	T4	AWS	T1	T3	T4	T1	T3	T4	T1	T3	T4
MAL	42.1	64.5	69.3	57.2	27.1 (5.9)	32.3 (6.5)	25.6 (4.5)	7.3 (5.1)	17.5 (8.2)	25.6 (4.2)	20.13 (8.3)	16.6 (5.5)	11.0 (3.7)
AIL	35.6	56.9	64.7	57.2	23.5 (6.7)	30.8 (6.4)	21.1 (4.1)	12.4 (6.9)	20.1 (10.0)	17.5 (3.0)	16.4 (9.3)	16.5 (4.0)	12.5 (3.7)
VAR	27.6	49.3	66	54.1	17.8 (3.9)	28.2 (2.9)	22.8 (3.2)	8.2 (3.7)	7.7 (2.8)	22.8 (3.4)	14.0 (9.5)	16.3 (4.7)	12.8 (3.5)
TII	29.1	60.8	61.8	53.6	18.0 (3.3)	22.2 (3.3)	16.3 (2.2)	3.8 (2.6)	21.3 (2.6)	9.4 (1.1)	14.2 (8.5)	13.7 (5.1)	10.0 (4.0)
PIS	22.3	54.2	51.1	52.8	10.1 (2.9)	19.0 (3.1)	11.8 (2.2)	4.3 (2.7)	16.7 (2.6)	4.9 (1.5)	6.4 (4.4)	13.2 (4.3)	9.0 (3.5)
HYY	26.1	61.3	54.7	45.4	11.5 (3.3)	20.7 (3.6)	16.7 (2.6)	3.4 (2.3)	12.8 (2.7)	5.6 (1.5)	7.9 (5.6)	15.4 (5.4)	13.1 (4.8)
KAR	28.5	52.1	48.4	37.6	12.0 (3.3)	17.8 (3.3)	12.7 (2.4)	4.2 (3.2)	11.1 (3.6)	5.4 (1.6)	8.2 (4.8)	11.4 (3.7)	10.7 (4.6)

3.3. Environmental drivers of the temperature variability

The performance of the monthly microclimate models was generally good but varied considerably across seasons and focus areas. The average model fit (R^2) for T1 was 0.44 (minimum R^2 was 0.00 and maximum 0.87), 0.50 (0.00–0.99) for T3, and 0.57 (0.00–0.99) for T4. On average, the Tmax models performed the best (0.53; 0.00–0.99), followed by Tavg (0.51; 0.05–0.96) and Tmin (0.49; 0.00–0.89). More detailed information about the R^2 values is presented in Fig S7 and Table S3.

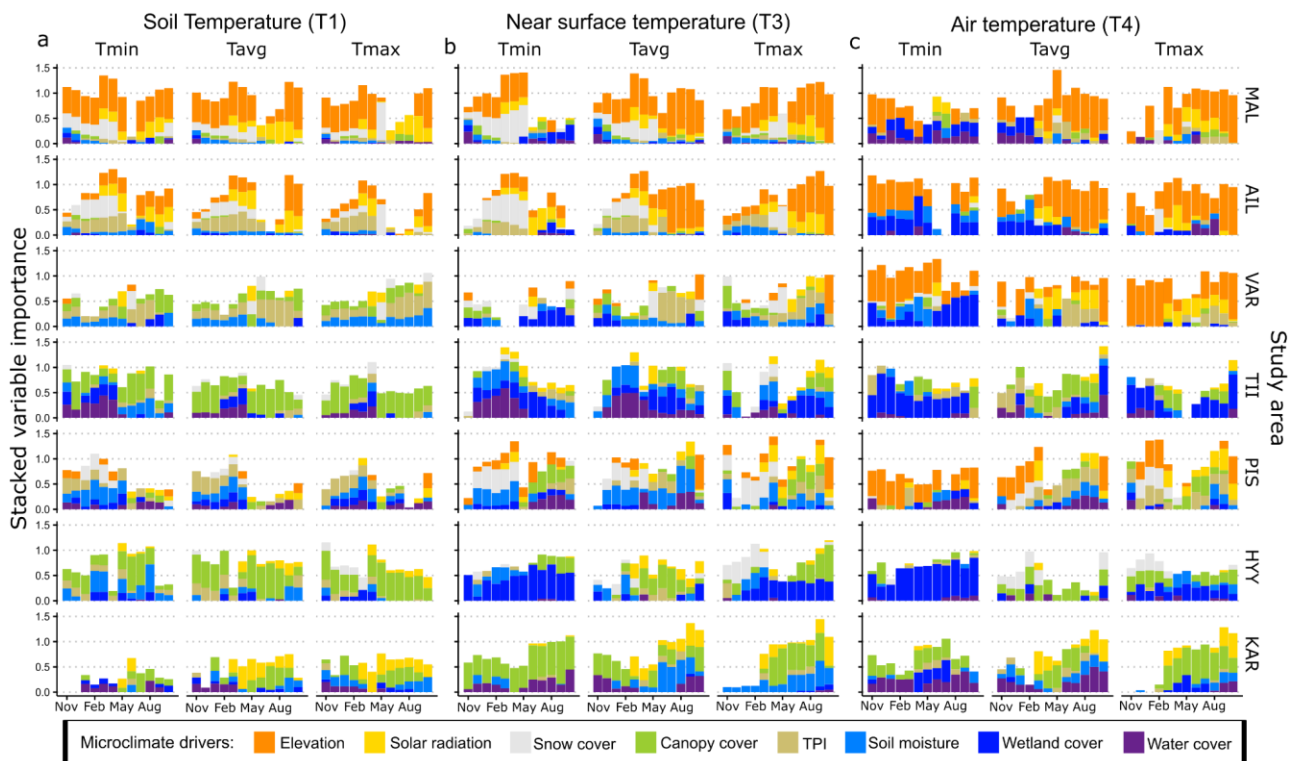Statistical modeling indicated that the drivers of microclimate temperatures vary across months and focus areas (Fig 5). Overall, canopy cover was identified as the most important variable in summer (May–August) and elevation in winter and shoulder seasons (September–April). In general, the relative importance of elevation and snow increased by latitude, whereas canopy cover had the largest influence in the southernmost focus areas. As expected, water-related variables were found to be important in study areas with extensive wetlands and lakes.

The direction of the effect of canopy cover on temperatures was dependent on measurement height, response variable, and season (Tables S4–S6). For example, in winter, soil temperatures

were consistently higher under closed canopies, whereas in summer the direction was reversed. In turn, T3 and T4 minimum temperatures were higher and maximum temperatures lower under canopies throughout the year, but for average temperatures the sign of the effect varied among seasons. Soil temperatures were consistently warmer under a thick snowpack (indicated by long snow cover duration), but during late spring, the sign of the effect turned opposite when slowly melting snow patches kept soil temperatures colder compared to the rest of the landscape. Snow also had a strong effect on near-surface temperatures by increasing Tmin and Tavg and decreasing Tmax. Elevation had, in general, a strong negative effect on temperatures, but especially minimum T4 temperatures showed strong contrasting effects throughout the year.

Figure 5. Relative influence of the environmental drivers explaining monthly microclimate temperature variability. Stacked variable importance scores of the predictors in monthly temperature models per temperature variable (Tmin, Tavg, Tmax) for the three

499   measurement heights (T1, T3, and T4) and for the seven study areas from north (MAL) to south

500   (KAR). Response variables in the models were the monthly minimum (Tmin), average (Tavg)

501   and maximum temperatures (Tmax). Height of the stacked bars also indicate the model fit i.e.,

502   a short bar means that the model explained only a little of the temperature variation. TPI =

503   Topographic position index.

504

505   4. Discussion

506   **4.1. Magnitude of thermal heterogeneity**

507   Our data revealed substantial spatio-temporal variations in microclimate temperatures with

508   distinct landscape and seasonal patterns. Overall, the largest variation in soil and air

509   temperatures was observed in the tundra, where local variability in topography, snow cover,

510   vegetation, and soil moisture create a fine-scale mosaic of thermal conditions (Daly et al., 2010;

511   Scherrer and Körner, 2011; Aalto et al., 2013; Niittynen et al., 2020). This high thermal

512   variability was poorly represented by adjacent AWS that often indicated lower ranges for air

513   temperatures compared to our measurements. Thus, these results provide support for the

514   argument that weather stations insufficiently capture the range of thermal conditions over

515   heterogeneous landscapes, which limits their usability in assessing local climate change

516   impacts (Graae et al., 2012; Lembrechts et al., 2019). We also found that thermal heterogeneity

517   within boreal and tundra landscapes varies markedly at monthly and shorter timescales, with

518   the largest instantaneous differences often exceeding 30°C near the ground (Fig 3). This

519   heterogeneity was particularly evident in the tundra in early summer during the time of partial

520   snow melt over the landscape. Similar patterns, but in smaller magnitudes, were also detectable

521   in soil temperatures. While the soil temperature heterogeneity during winter was relatively low,

522   the near-surface heterogeneity remained high during winter over most focus areas. This is likely

523   due to fine-scale variation in snow accumulation, which in the studied tundra systems is related

524 to complex topography and in boreal forests to canopy interception (Hedstrom and Pomeroy,

525 1998; Niittynen et al., 2020). As microclimate is typically not examined over different

526 environments and large extents, these thermal differences have remained undetected (Aalto et

527 al., 2013; Kemppinen et al., 2021). However, our comprehensive study design covering broad

528 geographical and environmental gradients enabled us to quantify the magnitude of thermal

529 heterogeneity and its drivers across distinct ecosystems and landscapes.

530

531 **4.2. Drivers of the microclimate temperatures**

532 Our results show that the main drivers of microclimate temperatures vary over landscapes and

533 seasons. For example, in the northernmost focus areas in the oroarctic tundra, the elevational

534 gradient clearly has the largest influence, especially on the above-surface temperatures via the

535 atmospheric lapse rate. Also, the role of local topography is particularly evident in the tundra,

536 where it drives microclimate temperature variability by controlling surface net radiation and

537 cold-air pooling (e.g., Daly et al., 2010; Dobrowski, 2011). In addition, local topography

538 controls spatial snow patterns and soil moisture, which are among the key factors creating

539 thermal heterogeneity close to the soil surface and controlling many ecosystem processes

540 (Aalto et al., 2013; le Roux et al., 2013; Niittynen et al., 2020). In our study design, local

541 elevational differences diminish towards the southernmost focus areas, and consequently, the

542 relative importance of other microclimate drivers increases. For example, our data reveal that

543 canopies, water bodies, and wetlands can create larger maximum and average thermal

544 heterogeneity in air temperatures in forests than observed in the tundra. Forest canopy is

545 especially important in the southernmost focus areas where dense canopies decrease the

546 maximum, but increase the minimum temperatures, which leads to buffered thermal conditions

547 compared to open areas.

548

549   Our data show that drivers of temperature variability are also dependent on the height from the

550   surface (De Frenne et al., 2021; Maclean and Klinges, 2021). This is demonstrated by the effect

551   of canopy cover – a dense canopy buffers air and near-surface temperature variation whereas

552   soil temperatures follow a distinct seasonal cycle where minimum, maximum, and mean

553   temperatures are all consistently lower in forests in summer but higher in winter compared to

554   open areas (in agreement with De Frenne et al., 2019). In our data, soil temperatures were

555   decoupled from elevational gradients, and, on average, elevation had the greatest importance

556   for air temperatures. This is especially evident in the tundra, where temperatures at >150 cm

557   are less affected by heterogeneous surface conditions and are more dependent on meso- and

558   macro-scale topographical gradients (Aalto et al., 2017; Maclean et al., 2019). During the study

559   period, temperature inversions in the lower atmosphere were so prevalent in our northernmost

560   focus areas that even the monthly mean air temperatures positively correlated with elevation

561   during some winter months. This is not evident in the near-surface temperatures recorded under

562   snow. In general, soil temperatures had similar driver contributions in minimum, maximum

563   and mean temperatures. Whereas, for near-surface and air temperatures, minimum and

564   maximum temperatures often had contrasting variable importances and effects. This is

565   probably because soil temperatures are less affected by short-term variability in weather and

566   radiation conditions, and thus, minimums and maximums are more closely coupled in soil

567   temperatures than in air (Ashcroft and Gollan, 2013). These height-dependent patterns that we

568   found highlight the importance of considering vertical temperature gradients when analyzing

569   microclimatic heterogeneity in space and time.

570

571   **4.3. Methodological uncertainties**

572   Statistical modeling of microclimates can be challenging, as the same variables and model

573   parameters proposed for one location and time may not be applicable for other areas and

574   seasons. Temperature variation follows physical principles but the commonly used geospatial

575   predictors are usually proxies for the underlying mechanisms (e.g., topographic position,

576   proximity to water bodies and wetlands). The quality and representativeness of such predictors

577   is crucial when interpreting the modeling results. Here, we aimed to evaluate the area-specific

578   strength of the statistical links between the predictors and the microclimate temperatures rather

579   than to produce accurate spatially explicit predictions. Most of the statistical relationships were

580   logical except for few individual results. For example, the models suggested that increasing

581   wetland cover decreased the minimum and increased the maximum air temperatures in our data

582   throughout the year, while in theory, a large water body should have the opposite effect,

583   especially during the snow and ice-free season. However, in our data the wetland cover was

584   negatively correlated with canopy cover in many of the focus areas (the smallest Spearman

585   correlation coefficient was -0.71), which may confound the found effects. Furthermore,

586   wetlands are typically located in topographic depressions, and thus, wetlands may be better

587   proxies for cold air pooling potential than a topographic position index (TPI). Mechanistic

588   microclimate models are increasingly developed and can solve some of these problems, but

589   they are similarly dependent on the input data quality and can also be computationally

590   demanding when applied over large extents at high spatial resolution (Maclean et al., 2019).

591   More research is needed to improve the quality of the geospatial data fed into statistical and

592   mechanistic microclimate models.

593

594   Measuring microclimate temperatures is prone to errors as the processes creating measurement

595   errors are the same as those responsible for creating the thermal variation (e.g., incoming solar

596   radiation, air mixing; Maclean et al., 2021). This is of particular concern for temperature

597   measurements conducted above the ground surface and if the sensors are exposed to sunlight.

598   Consequently, the sensors themselves can heat up, and the temperature recordings of ambient

599   conditions can be substantially overestimated. Radiation shielding around the sensors is

600   commonly used to mitigate the issue, but the choice of shielding (e.g., material, structure) is

601   not trivial (Maclean et al., 2021). In future studies, these measurement errors could be

602   accounted for by, for instance, quantifying the possible errors across seasons (e.g., snow

603   covered and bare ground), landscapes (contrasting expositions), and weather conditions.

604   Solving such practical methodological challenges is especially timely as new microclimate

605   networks are emerging (e.g., Greiser et al., 2018; Lembrechts et al., 2020) to facilitate more

606   accurate predictions of future microclimates and associated ecosystem impacts.

607

608   **4.4. Future microclimate temperatures and ecosystem implications**

609   Since the preindustrial time, the macroclimate has warmed 2.3°C over the study domain with

610   pronounced observed and predicted changes in thermal seasons, precipitation, and snow cover

611   (Mikkonen et al., 2015; Bintanja and Andry, 2017; Ruosteenoja et al., 2016, 2019; Luomaranta

612   et al., 2019). However, microclimates may not directly follow changes in macroclimate due to

613   the differing dynamics of the environmental drivers and how they are structured over

614   landscapes (e.g., Maclean et al., 2016; Aalto et al., 2018; De Frenne et al., 2019). For example,

615   elevation gradients and local topography as static drivers will create thermal heterogeneity also

616   in the future (Daly et al., 2010; Dobrowski, 2011). In turn, climate warming has already delayed

617   lake freeze-up and advanced ice break-up (Newton and Mullan, 2021), which can affect

618   microclimates of adjacent areas due to prolonged ice-free periods that sustain the energy

619   exchange between lake and atmosphere (Brown and Duguay, 2010). Changes in wetlands'

620   water balance (due to drainage and restoration) influence their thermal properties, energy

621   fluxes, and biogeophysical feedbacks that can lead to altered local temperature variability

622   (Menberu et al., 2016; Laine et al., 2019; Fernández-Pascual and Correia-Álvarez, 2021;

623   Słowińska et al., 2022). In the tundra, changes in snow cover and properties control temporal

624 dynamics and magnitude of landscape level thermal heterogeneity, especially close to the soil

625 surface (Aalto et al., 2018; Niittynen et al., 2020). Thus, shortening of the snow season could

626 translate into earlier peaks in landscape thermal heterogeneity and a general shift towards more

627 thermally homogeneous tundra landscapes. In both biomes, abiotic and biotic disturbances,

628 such as windstorms, wildland fires, and pest outbreaks, can lead to changes in local

629 temperatures due to their effect on e.g., vegetation structuring that in turn controls many of the

630 microclimatic processes (Venäläinen et al., 2020; De Frenne et al., 2021).

631

632 Microclimates and their changes have implications for the ecology and functioning of boreal

633 and tundra environments due to the inherent linkages to the organisms' performance and

634 ecosystem processes (Maclean et al., 2016; Körner and Hiltbrunner, 2018; Bentz et al. 2019;

635 Zellweger et al., 2020; Seibold et at., 2021). However, mostly due to a lack of observation data

636 such links have been anticipated rather than directly detected (De Frenne and Verheyen, 2016).

637 It is only with contemporary developments in data loggers and remote sensing that extensive

638 mapping of microclimates has become a reality (Lenoir et al., 2017; Zellweger et al., 2019).

639 Using microclimate data will allow more organism-centered approaches to determine species

640 range boundaries and related climate change dynamics (Potter et al., 2013; Bentz et al., 2019).

641 For example, microclimate could be incorporated into investigations of the temperature-driven

642 leading and trailing edges, where species' responses may be susceptible to the availability of

643 suitable microclimate and associated microrefugia (Hylander et al., 2015; Keppel et al., 2015).

644 Moreover, a landscape with various microclimates is also likely to transition slower to an

645 alternate state, whereas a landscape with homogeneous microclimate may transition due to

646 minor temperature shifts in the macroclimate (Randin et al., 2009; Lenoir et al., 2013; Aalto et

647 al., 2018). Therefore, thermally heterogeneous landscapes could be more resilient against

648 climate changes and short-term climate extremes (e.g., drought), and recover faster and/or

649 persist better in response to perturbations than their low resilience counterparts (Kühsel and

650 Blüthgen, 2015). With further expansions, our comprehensive study setting could also provide

651 possibilities to analyze, model, and compare the effects of microclimate on ecosystem

652 functioning of pristine and managed boreal forests. This is relevant, since different forest types

653 and management practices can produce substantial near-ground microclimate variation (De

654 Frenne and Verheyen, 2016; Greiser et al., 2018).

655

656 5. Conclusions

657 We showed remarkable multi-level microclimate temperature variability over boreal forest and

658 tundra biomes based on the data from hundreds of microclimate stations. The data revealed

659 high instantaneous thermal heterogeneity over the landscapes, with the largest differences

660 found in the tundra during wintertime and in southern boreal forest during summer. Our results

661 suggested that microclimate temperature variability in southern boreal forests is mostly driven

662 by canopy cover and proximity of water covers. In the tundra, the microclimatic temperature

663 variability is most strongly linked to the elevation gradient, variations in topographic solar

664 radiation and snow cover. Here we have also showed that the relative importance and effects

665 of microclimate drivers and landscape thermal heterogeneity vary seasonally. This calls for

666 careful investigation of the temporal aspects in future microclimate studies. As microclimate

667 temperatures are the most proximally related to organisms' performance and various ecosystem

668 functions, our new comprehensive data will be highly relevant in various ecosystem

669 applications aiming to understand and project the biome-wide responses to contemporary

670 climate change.

671

Conflict of interest

The authors declare no conflict of interests.

692   6. Literature cited

693   Aalto, J., le Roux, P. C., & Luoto, M. (2013). Vegetation mediates soil temperature and

694   moisture in arctic-alpine environments. Arctic, Antarctic, and Alpine Research, 45(4), 429–

695   439. https://doi.org/10.1657/1938-4246-45.4.429

696   Aalto, J., Riihimäki, H., Meineri, E., Hylander, K., & Luoto, M. (2017). Revealing topoclimatic

697   heterogeneity using meteorological station data. International Journal of Climatology,

698   37(S1), 544–556. https://doi.org/10.1002/joc.5020

699   Aalto, J., Scherrer, D., Lenoir, J., Guisan, A., & Luoto, M. (2018). Biogeophysical controls on

700   soil-atmosphere thermal differences: Implications on warming Arctic ecosystems.

701   Environmental Research Letters, 13(7), 074003. https://doi.org/10.1088/1748-9326/aac83e

702   Ashcroft, M. B., & Gollan, J. R. (2013). Moisture, thermal inertia, and the spatial distributions

703   of near-surface soil and air temperatures: Understanding factors that promote microrefugia.

704   Agricultural   and   Forest   Meteorology,   176,   77–89.   https://doi-

705   org.libproxy.helsinki.fi/10.1016/j.agrformet.2013.03.008

706   Barry, R., & Blanken, P. (2016). Microclimate and Local Climate. Cambridge University Press,

707   Cambridge.

708   Bedia, J., Herrera, S., & Gutiérrez, J. M. (2013). Dangers of using global bioclimatic datasets

709   for ecological niche modeling. Limitations for future climate projections. Global and

710   Planetary Change, 107, 1-12. https://doi.org/10.1016/j.gloplacha.2013.04.005

711   Bentz, B. J., Jönsson, A. M., Schroeder, M., Weed, A., Wilcke, R. A. I., & Larsson, K. (2019).

712   *Ips typographus* and *Dendroctonus ponderosae* models project thermal suitability for intra-

713   and inter-continental establishment in a changing climate. Frontiers in Forest and Global

714   Change 2(1). https://doi.org/10.3389/ffgc.2019.00001

715   Bintanja, R., & Andry, O. (2017). Towards a rain-dominated Arctic. Nature Climate Change,

716   7(4), 263-267. https://doi.org/10.1038/nclimate3240

717   Brown, L. C., & Duguay, C. R. (2010). The response and role of ice cover in lake-climate

718   interactions. Progress in physical geography, 34(5), 671-704. https://doi-

719   org/10.1177/0309133310375653

720   Daly, C., Conklin, D. R., & Unsworth, M. H. (2010). Local atmospheric decoupling in complex

721   topography alters climate change impacts. International Journal of Climatology, 30(12),

722   1857–1864. https://doi.org/10.1002/joc.2007

723   De Frenne, P., & Verheyen, K. (2016). Weather stations lack forest data. Science, 351(6270),

724   234-234. https://doi.org/10.1126/science.351.6270.234-a

725   De Frenne, P., Zellweger, F., Rodríguez-Sánchez, F., Scheffers, B. R., Hylander, K., Luoto,

726   M., Vellend, M., Verheyen, K., & Lenoir, J. (2019). Global buffering of temperatures under

727   forest canopies. Nature Ecology & Evolution, 3(5), 744–749.

728   https://doi.org/10.1038/s41559-019-0842-1

729   De Frenne, P., Lenoir, J., Luoto, M., Scheffers, B. R., Zellweger, F., Aalto, J., Ashcroft, M. B.,

730   Christiansen, D. M., Decocq, G., Pauw, K. D., Govaert, S., Greiser, C., Gril, E., Hampe, A.,

731   Jucker, T., Klinges, D. H., Koelemeijer, I. A., Lembrechts, J. J., Marrec, R., … & Hylander,

732   K. (2021). Forest microclimates and climate change: Importance, drivers and future research

733   agenda. Global Change Biology, 27(11), 2279–2297. https://doi.org/10.1111/gcb.15569

734   Dobrowski, S. Z. (2011). A climatic basis for microrefugia: The influence of terrain on climate.

735   Global Change Biology, 17(2), 1022–1035. https://doi.org/10.1111/j.1365-

736   2486.2010.02263.x

737   Du, E., Terrer, C., Pellegrini, A. F., Ahlström, A., van Lissa, C. J., Zhao, X., Xia, N., Wu, X.,

738   & Jackson, R. B. (2020). Global patterns of terrestrial nitrogen and phosphorus limitation.

739   Nature Geoscience, 13, 221-226. https://doi.org/10.1038/s41561-019-0530-4

740   Fernández-Pascual, E., & Correia-Álvarez, E. (2021). Mire microclimate: Groundwater buffers

741   temperature in waterlogged versus dry soils. International Journal of Climatology, 41(S1),

742   E2949–E2958. https://doi.org/10.1002/joc.6893

743   Fick, S. E., & Hijmans, R. J. (2017). WorldClim 2: new 1km spatial resolution climate surfaces

744   for global land areas. International Journal of Climatology, 37(12), 4302-4315.

745   https://doi.org/10.1002/joc.5086

746   Flato, G. M. (2011). Earth system models: An overview. Wiley Interdisciplinary Reviews:

747   Climate Change, 2(6), 783-800. https://doi.org/10.1002/wcc.148

748   Gardner, A. S., Maclean, I. M. D., & Gaston, K. J. (2019). Climatic predictors of species

749   distributions neglect biophysiologically meaningful variables. Diversity and Distributions,

750   25(8), 1318–1333. https://doi.org/10.1111/ddi.12939

751   Graae, B. J., De Frenne, P., Kolb, A., Brunet, J., Chabrerie, O., Verheyen, K., Pepin, N.,

752   Heinken, T., Zobel, M., & Shevtsova, A. (2012). On the use of weather data in ecological

753   studies along altitudinal and latitudinal gradients. Oikos, 121(1), 3–19.

754   https://doi.org/10.1111/j.1600-0706.2011.19694.x

755   Greenwell, B. M., & Boehmke, B. C. (2020). Variable Importance Plots—An Introduction to

756   the vip Package. The R Journal, 12(1), 343–366. https://doi.org/10.32614/RJ-2020-013

757   Greiser, C., Meineri, E., Luoto, M., Ehrlén, J., & Hylander, K. (2018). Monthly microclimate

758   models in a managed boreal forest landscape. Agricultural and Forest Meteorology, 250,

759   147–158. https://doi.org/10.1016/j.agrformet.2017.12.252

760   Grundstein, A., Todhunter, P., & Mote, T. (2005). Snowpack control over the thermal offset of

761   air and soil temperatures in eastern North Dakota. Geophysical Research Letters, 32(8).

762   https://doi.org/10.1029/2005GL022532

763   Haesen, S., Lembrechts, J. J., De Frenne, P., Lenoir, J., Aalto, J., Ashcroft, M. B., Kopecký,

764   M., Luoto, M., Maclean, I. M. D., Nijs, I., Niittynen, P., van den Hoogen, J., Arriga, N.,

765   Brůna, J., Buchmann, N., Čiliak, M., Collalti, A., De Lombaerde, E., Descombes, P., … Van

766   Meerbeek, K. (2021). ForestTemp – Sub-canopy microclimate temperatures of European

767   forests. Global Change Biology, 27(23), 6307-6319. https://doi.org/10.1111/gcb.15892

768   Hattab, T. & Lenoir, J. (2017). iSDM: Invasive Species Distribution Modelling. R package

769   version 1.0. https://CRAN.R-project.org/package=iSDM

770   Hedstrom, N. R., & Pomeroy, J. W. (1998). Measurements and modelling of snow interception

771   in   the   boreal   forest.   Hydrological   Processes,   12(10-11),   1611-1625.

772   https://doi.org/10.1002/(SICI)1099-1085(199808/09)12:10/11<1611::AID-

773   HYP684>3.0.CO;2-4

774   Hylander, K., Ehrlén, J., Luoto, M., & Meineri, E. (2015). Microrefugia: Not for everyone.

775   Ambio, 44(1), 60-68. https://doi.org/10.1007/s13280-014-0599-3

776   Jokinen, P., Pirinen, P., Kaukoranta, J.-P., Kangas, A., Alenius, P., Eriksson, P., Johansson,

777   M., & Wilkman, S. (2021). Tilastoja Suomen ilmastosta ja merestä 1991-2020. Ilmatieteen

778   laitos – Finnish Meteorological Institute, Raportteja 2021:8.

779   Karger, D. N., Conrad, O., Böhner, J., Kawohl, T., Kreft, H., Soria-Auza, R. W., Zimmermann,

780   N. E., Linder, P., & Kessler, M. (2017). Climatologies at high resolution for the Earth land

781   surface areas. Scientific Data, 4(1), 1-12. https://doi.org/10.1038/sdata.2017.122

782   Kemppinen, J., Niittynen, P., Virkkala, A.-M., Happonen, K., Riihimäki, H., Aalto, J., & Luoto,

783   M. (2021). Dwarf shrubs impact tundra soils: drier, colder, and less organic carbon.

784   Ecosystems, 24(6), 1378-1392. https://doi.org/10.1007/s10021-020-00589-2

785   Keppel, G., Mokany, K., Wardell-Johnson, G. W., Phillips, B. L., Welbergen, J. A., & Reside,

786   A. E. (2015). The capacity of refugia for conservation planning under climate change.

787   Frontiers in Ecology and the Environment, 13(2), 106–112. https://doi.org/10.1890/140055

788   Körner, C., & Hiltbrunner, E. (2018). The 90 ways to describe plant temperature. Perspectives

789   in   Plant   Ecology,   Evolution   and   Systematics,   30,   16–21.

790   https://doi.org/10.1016/j.ppees.2017.04.004

791   Kühsel, S., & Blüthgen, N. (2015). High diversity stabilizes the thermal resilience of pollinator

792   communities in intensively managed grasslands. Nature communications, 6(1), 1-10.

793   https://doi.org/10.1038/ncomms8989

794   Laine, A. M., Mehtätalo, L., Tolvanen, A., Frolking, S., & Tuittila, E.-S. (2019). Impacts of

795   drainage, restoration and warming on boreal wetland greenhouse gas fluxes. Science of The

796   Total Environment, 647, 169–181. https://doi.org/10.1016/j.scitotenv.2018.07.390

797   Lembrechts, J. J., Lenoir, J., Roth, N., Hattab, T., Milbau, A., Haider, S., Pellissier, L.,

798   Pauchard, A., Ratier Backes, A., Dimarco, R. D., Nuñez, M. A., Aalto, J., & Nijs, I. (2019).

799   Comparing temperature data sources for use in species distribution models: From in-situ

800   logging to remote sensing. Global Ecology and Biogeography, 28(11), 1578–1596.

801   https://doi.org/10.1111/geb.12974

802   Lembrechts, J. J., Aalto, J., Ashcroft, M. B., De Frenne, P., Kopecký, M., Lenoir, J., Luoto,

803   M., Maclean, I. M. D., Roupsard, O., Fuentes-Lillo, E., García, R. A., Pellissier, L.,

804   Pitteloud, C., Alatalo, J. M., Smith, S. W., Björk, R. G., Muffler, L., Ratier Backes, A.,

805   Cesarz, S., … Nijs, I. (2020). SoilTemp: A global database of near-surface temperature.

806   Global Change Biology, 26(11), 6616–6629. https://doi.org/10.1111/gcb.15123

807   Lenoir, J., Graae, B. J., Aarrestad, P. A., Alsos, I. G., Armbruster, W. S., Austrheim, G.,

808   Bergendorff, C., Birks, H. J. B., Bråthen, K. A., Brunet, J., Bruun, H. H., Dahlberg, C. J.,

809   Decocq, G., Diekmann, M., Dynesius, M., Ejrnaes, R., Grytnes, J.-A., Hylander, K.,

810   Klanderud, K., … & Svenning, J.-C. (2013). Local temperatures inferred from plant

811   communities suggest strong spatial buffering of climate warming across Northern Europe.

812   Global Change Biology, 19(5), 1470–1481. https://doi.org/10.1111/gcb.12129

813 Lenoir, J., Hattab, T., & Pierre, G. (2017). Climatic microrefugia under anthropogenic climate

814 change: Implications for species redistribution. Ecography, 40(2), 253-266.

815 https://doi.org/10.1111/ecog.02788

816 Luomaranta, A., Aalto, J., & Jylhä, K. (2019). Snow cover trends in Finland over 1961–2014

817 based on gridded snow depth observations. International Journal of Climatology, 39(7),

818 3147–3159. https://doi.org/10.1002/joc.6007

819 Maclean, I. M. D., Suggitt, A. J., Wilson, R. J., Duffy, J. P., & Bennie, J. J. (2016). Fine-scale

820 climate change: Modelling spatial variation in biologically meaningful rates of warming.

821 Global Change Biology, 23(1), 256-268. https://doi.org/10.1111/gcb.13343

822 Maclean, I. M. D., Mosedale, J. R., & Bennie, J. J. (2019). Microclima: An R package for

823 modelling meso- and microclimate. Methods in Ecology and Evolution, 10, 280-290.

824 https://doi.org/10.1111/2041-210X.13093

825 Maclean, I. M. D., Duffy, J. P., Haesen, S., Govaert, S., De Frenne, P., Vanneste, T., Lenoir,

826 J., Lembrechts, J. J., Rhodes, M. W., & Van Meerbeek, K. (2021). On the measurement of

827 microclimate. Methods in Ecology and Evolution, 12(8), 1397–1410.

828 https://doi.org/10.1111/2041-210X.13627

829 Maclean, I. M. D., & Klinges, D. H. (2021). Microclimc: A mechanistic model of above, below

830 and within-canopy microclimate. Ecological Modelling, 451, 109567.

831 https://doi.org/10.1016/j.ecolmodel.2021.109567

832 McGuire, A. D., Anderson, L. G., Christensen, T. R., Dallimore, S., Guo, L., Hayes, D. J.,

833 Heimann, M., Lorenson, T. D., Macdonald, R. W., & Roulet, N. (2009). Sensitivity of the

834 carbon cycle in the Arctic to climate change. Ecological Monographs, 79(4), 523-555.

835 https://doi.org/10.1890/08-2025.1

836 Menberu, M. W., Tahvanainen, T., Marttila, H., Irannezhad, M., Ronkanen, A.-K., Penttinen,

837 J., & Kløve, B. (2016). Water-table-dependent hydrological changes following peatland

838   forestry drainage and restoration: Analysis of restoration success. Water Resources

839   Research, 52(5), 3742–3760. https://doi.org/10.1002/2015WR018578

840   Mikkonen, S., Laine, M., Mäkelä, H. M., Gregow, H., Tuomenvirta, H., Lahtinen, M., &

841   Laaksonen, A. (2015). Trends in the average temperature in Finland, 1847–2013. Stochastic

842   Environmental Research and Risk Assessment, 29(6), 1521-1529.

843   https://doi.org/10.1007/s00477-014-0992-2

844   Newton, A. M. W., & Mullan, D. J. (2021). Climate change and Northern Hemisphere lake and

845   river ice phenology from 1931–2005. The Cryosphere, 15(5), 2211–2234.

846   https://doi.org/10.5194/tc-15-2211-2021

847   Niittynen, P., Heikkinen, R. K., Aalto, J., Guisan, A., Kemppinen, J., & Luoto, M. (2020). Fine-

848   scale tundra vegetation patterns are strongly related to winter thermal conditions. Nature

849   Climate Change, 10(12), 1143–1148. https://doi.org/10.1038/s41558-020-00916-4

850   Pepin, N. C., Schaefer, M. K., & Riddy, L. D. (2009). Quantification of the cold-air pool in

851   Kevo Valley, Finnish Lapland. Weather, 64(3), 60–67. https://doi.org/10.1002/wea.260

852   Post, E., Forchhammer, M. C., Bret-Harte, M. S., Callaghan, T. V., Christensen, T. R.,

853   Elberling, B., Fox, A. D., Gilg, O., Hik, D. S., Høye, T. T., Ims, R. A., Jeppesen, E., Klein,

854   D. R., Madsen, J., McGuire, A. D., Rysgaard, S., Schindler, D. E., Stirling, I., Tamstorf, M.

855   P., … & Aastrup, P. (2009). Ecological dynamics across the Arctic associated with recent

856   climate change. Science 325, 1355–1358. https://doi.org/10.1126/science.1173113

857   Potter, K. A., Woods, H. A., & Pincebourde, S. (2013). Microclimatic challenges in global

858   change biology. Global Change Biology, 19(10), 2932–2939.

859   https://doi.org/10.1111/gcb.12257

860   Randin, C. F., Engler, R., Normand, S., Zappa, M., Zimmermann, N. E., Pearman, P. B., Vittoz,

861   P., Thuiller, W., & Guisan, A. (2009). Climate change and plant distribution: local models

862   predict high-elevation persistence. Global Change Biology, 15(6), 1557-1569.
863   https://doi.org/10.1111/j.1365-2486.2008.01766.x

864   Roussel, J.-R., Auty, D., Coops, N. C., Tompalski, P., Goodbody, T. R. H., Meador, A. S.,
865   Bourdon, J.-F., de Boissieu, F., & Achim, A. (2020). lidR: An R package for analysis of
866   Airborne Laser Scanning (ALS) data. Remote Sensing of Environment, 251, 112061.
867   https://doi.org/10.1016/j.rse.2020.112061

868   Ruosteenoja, K., Jylhä, K., & Kämäräinen, M. (2016). Climate Projections for Finland Under
869   the RCP Forcing Scenarios. Geophysica, 51(1), 17-50.

870   Ruosteenoja, K., Markkanen, T., & Räisänen, J. (2019). Thermal seasons in northern Europe
871   in projected future climate. International Journal of Climatology 40(10), 4444-4462.
872   https://doi.org/10.1002/joc.6466

873   le Roux, P. C., Aalto, J., & Luoto, M. (2013). Soil moisture's underestimated role in climate
874   change impact modelling in low-energy systems. Global Change Biology, 19(10), 2965-
875   2975. https://doi.org/10.1111/gcb.12286

876   Scherrer, D., & Koerner, C. (2011). Topographically controlled thermal-habitat differentiation
877   buffers alpine plant diversity against climate warming. Journal of Biogeography, 38(2),
878   406–416. https://doi.org/10.1111/j.1365-2699.2010.02407.x

879   Seibold, S., Rammer, W., Hothorn, T., Seidl, R., Ulyshen, M. D., Lorz, J., Cadotte, M. W.,
880   Lindenmayer, D. B., Adhikari, Y. P., Aragón, R., Bae, S., Baldrian, P., Barimani Varandi,
881   H., Barlow, J., Bässler, C., Beauchêne, J., Berenguer, E., Bergamin, R. S., Birkemoe, T., …,
882   & Müller, J. (2021). The contribution of insects to global forest deadwood decomposition.
883   Nature, 597(7874), 77–81. https://doi.org/10.1038/s41586-021-03740-8

884   Słowińska, S., Słowiński, M., Marcisz, K., & Lamentowicz, M. (2022). Long-term
885   microclimate study of a peatland in Central Europe to understand microrefugia.
886   International Journal of Biometeorology. https://doi.org/10.1007/s00484-022-02240-2

887   Soudzilovskaia, N. A., van der Heijden, M. G., Cornelissen, J. H., Makarov, M. I., Onipchenko,

888   V. G., Maslov, M. N., Akhmetzhanova, A. A., & van Bodegom, P. M. (2015). Quantitative

889   assessment of the differential impacts of arbuscular and ectomycorrhiza on soil carbon

890   cycling. New Phytologist, 208(1), 280-293. https://doi.org/10.1111/nph.13447

891   Suggitt, A. J., Gillingham, P. K., Hill, J. K., Huntley, B., Kunin, W. E., Roy, D. B., & Thomas,

892   C. D. (2011). Habitat microclimates drive fine-scale variation in extreme temperatures.

893   Oikos, 120(1), 1–8. https://doi.org/10.1111/j.1600-0706.2010.18270.x

894   Tikkanen, M. (2005). Climate. In: Seppälä, M. (eds): The physical geography of Fennoscandia.

895   Oxford University Press, Oxford.

896   Venäläinen, A., Lehtonen, I., Laapas, M., Ruosteenoja, K., Tikkanen, O.-P., Viiri, H., Ikonen,

897   V.-P., & Peltola, H. (2020). Climate change induces multiple risks to boreal forests and

898   forestry in Finland: A literature review. Global Change Biology, 26(8), 4178–4196.

899   https://doi.org/10.1111/gcb.15183

900   Virkkala, A.-M., Aalto, J., Rogers, B. M., Tagesson, T., Treat, C. C., Natali, S. M., Watts, J.

901   D., Potter, S., Lehtonen, A., Mauritz, M., Schuur, E. A. G., Kochendorfer, J., Zona, D.,

902   Oechel, W., Kobayashi, H., Humphreys, E., Goeckede, M., Iwata, H., Lafleur, P. M., … &

903   Luoto, M. (2021). Statistical upscaling of ecosystem CO2 fluxes across the terrestrial tundra

904   and boreal domain: Regional patterns and uncertainties. Global Change Biology, 27(17),

905   4040–4059. https://doi.org/10.1111/gcb.15659

906   Wild, J., Kopecký, M., Macek, M., Šanda, M., Jankovec, J., & Haase, T. (2019). Climate at

907   ecologically relevant scales: A new temperature and soil moisture logger for long-term

908   microclimate measurement. Agricultural and Forest Meteorology, 268, 40-47.

909   https://10.1016/j.agrformet.2018.12.018

910   Yang, Z., Hanna, E., Callaghan, T. V., & Jonasson, C. (2012). How can meteorological

911   observations and microclimate simulations improve understanding of 1913–2010 climate

912   change around Abisko, Swedish Lapland? Meteorological Applications, 19(4), 454–463.

913   https://doi.org/10.1002/met.276

914   Zellweger, F., De Frenne, P., Lenoir, J., Rocchini, D., & Coomes, D. (2019). Advances in

915   microclimate ecology arising from remote sensing. Trends in Ecology & Evolution, 34(4),

916   327-341. https://doi-org.libproxy.helsinki.fi/10.1016/j.tree.2018.12.012

917   Zellweger, F., De Frenne, P., Lenoir, J., Vangansbeke, P., Verheyen, K., Bernhardt-

918   Römermann, M., Baeten, L., Hédl, R., Berkl, I., Brunet, J., van Calster, H., Chudomelová,

919   M., Decocq, G., Dirnböck, T., Durak, T., Heinken, T., Jaroszewicz, B., Kopecký, M., Máliš,

920   F., ... & Coomes, D. (2020). Forest microclimate dynamics drive plant responses to

921   warming. Science, 368(6492), 772-775. https://doi.org/10.1126/science.aba6880